Observing parity-time symmetry breaking in a Josephson parametric amplifier

Chandrashekhar Gaikwad , 1,* Daria Kowsari , 1,2,3 Weijian Chen , 1 and Kater W. Murch 1 Department of Physics, Washington University, St. Louis, Missouri 63130, USA
2 Department of Physics and Astronomy, Dornsife College of Letters, Arts, and Sciences,
University of Southern California, Los Angeles, California 90089, USA
3 Center for Quantum Information Science and Technology, University of Southern California, Los Angeles, California 90089, USA

(Received 22 June 2023; revised 3 October 2023; accepted 9 October 2023; published 13 November 2023)

A coupled two-mode system with balanced gain and loss is a paradigmatic example of an open quantum system that can exhibit real spectra despite being described by a non-Hermitian Hamiltonian. We utilize a degenerate parametric amplifier operating in three-wave mixing mode to realize such a system of balanced gain and loss between the two quadrature modes of the amplifier. By examining the time-domain response of the amplifier, we observe a characteristic transition from real-to-imaginary energy eigenvalues associated with the parity-time symmetry breaking transition.

DOI: 10.1103/PhysRevResearch.5.L042024

Parity-time (PT) symmetry was introduced as a compelling paradigm for open quantum systems described by non-Hermitian Hamiltonians that can still have real energy spectra [1]. Originally introduced in the context of complex potentials, the study of PT symmetry has taken on important relevance due to progress in optics [2]. A paradigmatic example for demonstrating PT symmetry consists of two coupled optical modes with balanced gain and loss. These PT dimers have been studied extensively in a range of experimental platforms [3–9]. Of particular interest are exceptional point (EP) degeneracies [10,11], which have been identified to confer interesting advantages and functionalities, such as enhanced sensitivity [12–14] and tuning capabilities [15]. Recently, there have been efforts to extend the study of exceptional points to the quantum domain with recent superconducting circuit experiments utilizing purely lossy dynamics to realize passive PT symmetry [16–19]. Alternatively, Hamiltonian dilation [20] can be used to simulate arbitrary Hamiltonians, a method that has been employed with nitrogen-vacancy centers [21,22]. In the quantum domain, amplification is constrained by the requirement that the commutation relation between operators is maintained—leading to fundamental limits for added quantum noise in amplifiers [23]. In particular, dissipation-free gain, and therefore noiseless amplification can be achieved in the context of squeezing—where one quadrature is amplified and its conjugate is deamplified, preserving the operator commutation relation. In this Letter, we investigate the realization of a PT-dimer system in this

Published by the American Physical Society under the terms of the Creative Commons Attribution 4.0 International license. Further distribution of this work must maintain attribution to the author(s) and the published article's title, journal citation, and DOI.

dissipation-free setting [24]. This goes beyond prior work where incoherent gain is associated with added noise. We utilize a parametric amplifier [25–27] operating in three-wave mixing mode, where the two quadratures of an electromagnetic mode are either amplified or squeezed, corresponding to the respective gain and loss in the PT-dimer model. A detuning between the pump frequency and the amplifier's resonance introduces coupling between the two quadratures, allowing us to observe the interplay between coupling and gain/loss that characterizes the PT symmetry breaking transition in the transient response of the amplifier. This observation opens the door to a new class of quantum microwave devices that harness non-Hermiticity and exceptional points for a variety of purposes including nonreciprocity [28], enhanced sensing [29,30], and the study of novel topological quantum materials [31-36].

The PT dimer is considered to be one of the simplest systems obeying PT symmetry, and has thus been studied in a diverse range of contexts [3–9,15–19,21,22]. As we depict in Fig. 1(a), the PT dimer consists of two modes, which we label A and B. The two modes are respectively subject to gain and loss given by rate $\gamma/2$. The system is invariant under the PT operation as the parity operator switches the modes A and B and time reversal exchanges gain and loss. The two modes are coupled at a rate g. The time evolution of the PT dimer is given by the equation of motion,

$$i\partial_t \binom{A}{B} = H_{PT} \binom{A}{B},\tag{1}$$

where

$$H_{PT} = \begin{pmatrix} +i\frac{\gamma}{2} & g \\ g & -i\frac{\gamma}{2} \end{pmatrix} = g\sigma_x + i\frac{\gamma}{2}\sigma_z.$$
 (2)

Examining the eigenvalues of H_{PT} ,

$$\lambda_{\pm} = \pm \sqrt{g^2 - (\gamma/2)^2},\tag{3}$$

^{*}chandrashekhar@wustl.edu

[†]murch@physics.wustl.edu

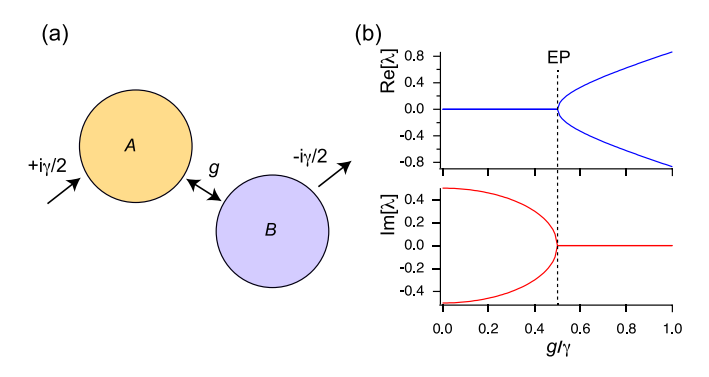


FIG. 1. The PT dimer. (a) The PT dimer consists of two coupled modes with respective gain and loss. (b) The complex eigenvalue spectrum of the PT dimer exhibits a transition from purely imaginary to purely real eigenvalues separated by an exceptional point. For the plot, $\gamma = 1$.

we can see that the coupling rate g can tune the system from a region of "unbroken" PT symmetry $(g > \gamma/2)$, where the eigenvalues are strictly real, to a region of "broken" PT symmetry $(g < \gamma/2)$, where the eigenvalues are purely imaginary. The real and imaginary parts of the eigenvalues are displayed in Fig. 1(b). The exceptional point is the degeneracy of the system and occurs at $g = \gamma/2$, where H_{PT} is not diagonalizable and there is a single eigenmode of the system.

The PT dimer exhibits many of the salient features of non-Hermitian systems. The tuning of the eigenvalues from real-to-imaginary regions corresponds to the "PT symmetry breaking transition." In the unbroken region, the dynamics are oscillatory, and in the broken region the dynamics are amplifying or deamplifying for the modes with respective gain or loss [16,21]. Near the exceptional point degeneracy, the eigenvalues depend sensitively on the control parameter g, leading to enhanced sensitivity [12–14] to a small perturbation δg . The eigenvectors of Eq. (2) can be written as

$$|\pm
angle \propto {\lambda_{\pm} \choose g},$$

which indicates how the eigenvectors are generally nonorthogonal, and coalesce at the EP. Finally, as parametrized in Eq. (2), there is only one relevant control parameter, yet if another parameter is included, the eigenvalues can be tuned to be complex rather than purely real or imaginary. In this case, the topology of the Riemann manifold that describes the complex energy becomes an interesting tuning landscape i.e. changing the control parameters enables encircling the EP, with intriguing features of nonreciprocity [15] and chiral behavior [19].

In this Letter, we utilize a Josephson parametric amplifier to realize the essential physics of the *PT* dimer. Josephson parametric amplifiers utilize nonlinearity imparted by Josephson junctions in a superconducting circuit to perform wave mixing between a strong classical pump and weak quantum signals [25]. These amplifiers are utilized broadly in the circuit quantum electrodynamics architecture [37,38] for achieving quantum noise limited amplification and have also been employed for research into quantum nonlinear dynamics [39,40]. Here, we focus on the case of three-wave mixing,

where one pump photon at frequency ω_p converts into one signal photon at frequency ω_s and one idler photon at frequency ω_i operating in degenerate mode, where the signal is degenerate with the idler ($\omega_s = \omega_i = \omega_p/2$). The Hamiltonian of such a parametric amplifier can be expressed in the rotating frame as [41]

$$H_{\rm DPA} = \delta a^{\dagger} a + \frac{\nu}{2} (i a^{\dagger 2} - i a^2), \tag{4}$$

where $\delta \equiv (\omega_{\rm p}/2 - \omega_0)$ is the detuning from the resonance of the amplifier at frequency ω_0 , ν is the pump strength, and a (a^{\dagger}) is the photon annihilation (creation) operator for photons at the signal frequency. The last two terms in the Hamiltonian imply the three-wave mixing process between two signal photons and one pump photon; since the pump drive is far stronger than any other signal involved in the system, it is treated as classical.

Even though the system consists of a single bosonic mode, a and a^{\dagger} are still coupled through the parametric drive and can be written in vector basis $|a\rangle = (a, a^{\dagger})^T$, where $(\cdot)^T$ represents the transpose operation. The Heisenberg equation of motion can be formally written as

$$i\partial_t |a\rangle = \begin{pmatrix} \delta & i\nu \\ i\nu & -\delta \end{pmatrix} |a\rangle.$$
 (5)

To illustrate the connection between the degenerate parametric amplifier and the PT dimer, we now transform to the quadrature basis $\{I=(a+a^{\dagger})/\sqrt{2},\ Q=(a-a^{\dagger})/i\sqrt{2}\}$. In this basis, the Heisenberg equation of motion is given by

$$i\partial_t \begin{pmatrix} I \\ iQ \end{pmatrix} = \begin{pmatrix} i\nu & \delta \\ \delta & -i\nu \end{pmatrix} \begin{pmatrix} I \\ iQ \end{pmatrix}. \tag{6}$$

This evolution matrix realizes the PT-dimer Hamiltonian Eq. (2). Here, the pump is the source of coherent gain and loss and the detuning is equivalent to the coupling. This system exhibits a PT transition when the threshold ($\delta = \nu$) is crossed. At $|\delta| > |\nu|$ the pump drive is too weak to pin the signal's phase hence the system exhibits oscillatory behavior in the two quadratures—corresponding to the PT symmetry unbroken regime. However, in the case of $|\delta| < |\nu|$, the pump is sufficient to give one quadrature gain while squeezing the other quadrature—corresponding to the PT symmetry broken regime.

So far, our discussion has focused on Hamiltonian dynamics, yet to probe the associated physics, an experimental device requires input and output ports. These will allow us to inject probe signals, and monitor the dynamics of the quadratures via a weakly coupled output port. Formally, the operator for the output mode is given $a_{\text{out}} = \sqrt{\kappa_{\text{out}}} a$, where κ_{out} is the coupling rate to the output port. Hence, the output quadratures ($I_{\text{out}}, Q_{\text{out}}$) will simply be proportional to the quadratures (I, Q) of the amplifier. Additionally, due to this dissipation of the output port, the associated dynamics will occur in the transient response of the amplifier as it evolves to a steady state.

We designed a narrow-bandwidth three-wave mixing amplifier. Figure 2(a) displays the photograph of the device which is patterned as a single-layer device with Josephson junctions formed from double-angle evaporated aluminum. The equivalent circuit schematic, shown in Fig. 2(b), displays a device with $C_a = 1.085$ pF capacitance, $L_a = 0.92$ nH linear

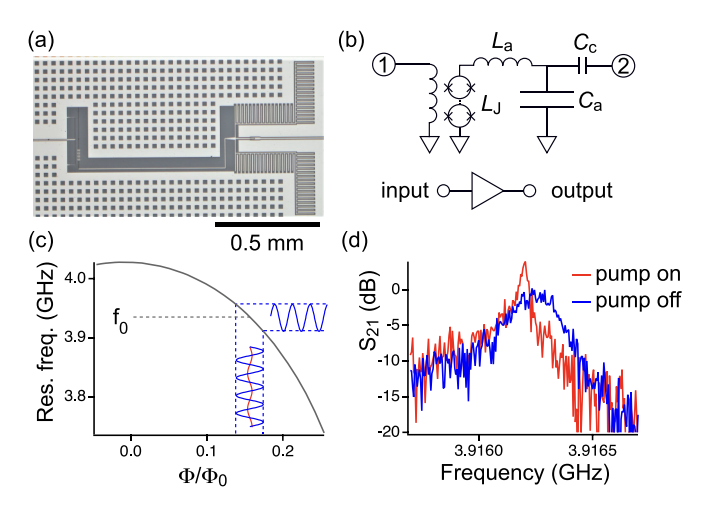


FIG. 2. Degenerate parametric amplifier. (a) Optical micrograph of the device. (b) Circuit schematic of the device; the input port (1) is used for both pump and signal inputs, and the output port (2) is used to monitor the amplifier dynamics. (c) The amplifier is flux biased to generate a first-order flux sensitivity to the pump. When pumped at ω_p , the amplifier frequency is modulated at ω_p . We probe the response of a small signal at frequency $\omega_s = \omega_p/2$. (d) The amplifier's frequency response exhibits enhanced transmission near the resonance frequency, with amplification above the response when the pump is turned on.

inductance, and $L_{\rm J}=0.516$ nH Josephson inductance. When coupled to the 50- Ω input/output port with a capacitance of $C_{\rm c}=84$ fF, the amplifier resonance frequency (without flux bias) is at 4.028 GHz with a quality factor of 20×10^3 . The Josephson inductance is realized as an array of four superconducting quantum interference devices (SQUIDs). The SQUID loop areas are $5.5\times5~\mu {\rm m}^2$, and the critical current of each SQUID is $3.2~\mu A$. A high-bandwidth microwave input line is coupled to the SQUID array with a mutual inductance of 80 pH, allowing the microwave drive to modulate $L_{\rm J}$ at twice the amplifier frequency. Additionally, residual capacitive coupling between the input line and the amplifier allows us to inject a small signal via this port.

The device is wire-bonded to a microwave circuit board and cooled to 20 mK and protected from magnetic flux and electromagnetic radiation with associated shielding. The pump port of the device is filtered and attenuated (total of 50 dB attenuation). The device output passes through two cryogenic circulators and is amplified by a high electron mobility transistor (HEMT) amplifier. We use an external coil to apply a dc flux bias to the system of approximately $\Phi_0/6$, where Φ_0 is the magnetic flux quantum. As is shown in Fig. 2(c), this flux bias results in a linear coupling between the pump and the amplifier, allowing the pump to modulate the Josephson inductance at the pump frequency.

We first characterize the amplifier response in the frequency domain. Figure 2(d) displays the transmission through the amplifier when the pump tone is off (no gain) and when it is set to achieve a gain of approximately 4.2 dB. The transmission exhibits a resonant response, with gain evident as an increase in the transmission.

At this point, we have introduced a narrow-bandwidth parametric amplifier that is optimized for examining the

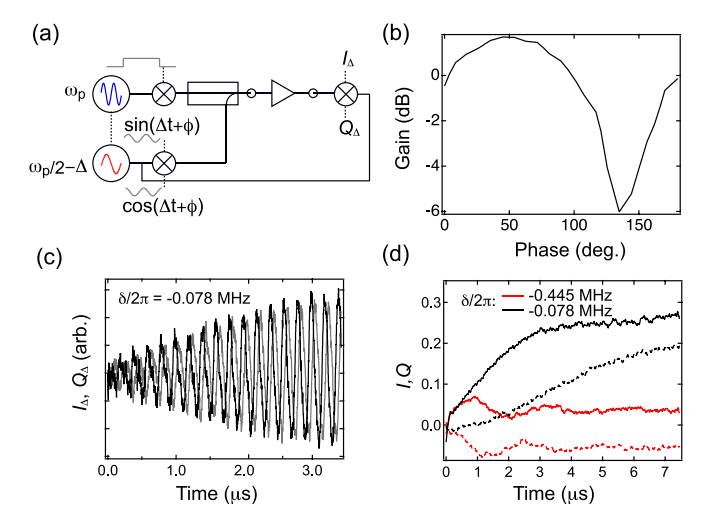


FIG. 3. Time-domain response. (a) The microwave setup includes a signal probe that is phase locked to the pump frequency (dashed line). Single-sideband modulation shifts the probe signal to be degenerate with the pump $\omega_s = \omega_p/2$. The output signal is demodulated. (b) The gain of the amplifier is phase sensitive; we sweep the phase of the probe signal so that one quadrature is amplified and the other is squeezed. (c) Time-domain response of I_{Δ} and Q_{Δ} where the signal and pump are turned on simultaneously. I_{Δ} and Q_{Δ} are demodulated to obtain I and Q. (d) The time evolution of I (solid) and Q (dashed) for two different values of the detuning.

interplay of gain/loss and coupling characteristic of the PT dimer. To probe the PT symmetry breaking transition, we now turn to the time-domain response of the amplifier. Figure 3(a) displays the microwave modulation/demodulation and timing of the experiment. We utilize two (pump, signal) microwave generators operating at ω_p and $\omega_s - \Delta = \omega_p/2 - \Delta$, which are interferometrically locked via frequency doubling and demodulation to maintain exquisite phase stability. The signal generator's tone is upconverted by Δ using single-sideband modulation and combined with the pump tone. Signals that are transmitted through the amplifier are demodulated at frequency $\omega_s - \Delta$, leading to heterodyne detection.

Since the amplifier is operated in degenerate mode $(2\omega_s = \omega_p)$, the amplification is phase sensitive, i.e., signals that are in phase with the pump are amplified, and signals that are in quadrature with the pump are deamplified. Figure 3(b) displays the amplifier transmission as the relative phase between the pump and signal is tuned, showing the characteristic response of phase-sensitive amplification. We choose the phase offset $\phi_0 = 45^\circ$ which corresponds to amplification of the input signal.

Figure 3(c) displays a representative time-domain response of the amplifier. At t=0 the probe signal and pump are turned on, and the demodulated and digitized quadratures show an increasing envelope with modulation at the heterodyne frequency $\Delta/2\pi=5$ MHz. We further demodulate this heterodyne signal to determine the quadratures I and Q. We use a Savitzky-Golay filter with a window size of 500 ns and polynomial order of 5 to smooth the data. In Fig. 3(d), we display the time response of I, Q for different choices of the detuning between the signal/pump and amplifier resonance. The evolution of (I, Q) exhibits a transition from oscillatory to saturated

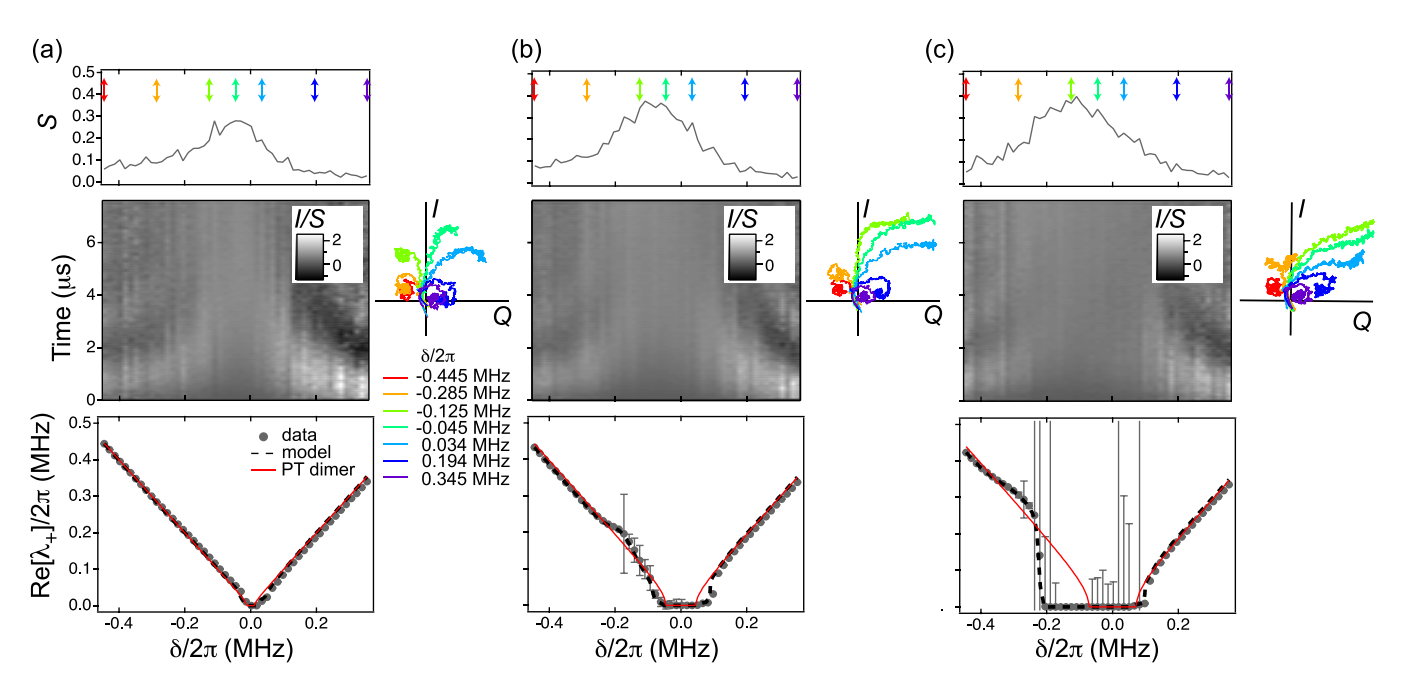


FIG. 4. PT symmetry breaking transition in a parametric amplifier. The graphs display the time response of I vs δ for three different pump strengths, increasing sequentially corresponding to $v/2\pi=0.013$ (a), 0.046 (b), and 0.072 (c) MHz. The grayscale plots are normalized to the steady state response (given by the value at a time duration of 7.6 μ s, shown in the top panel). The side panels display the time evolution of I of I a time duration of 7.512 I I is. The lower panels display the extracted frequency from the transient response (markers). The error bars represent estimated errors of the fits and the dashed line gives the fit of the model's data. The red curves indicate the eigenvalues of the I I I dimer Hamiltonian [Eq. (6)]. A clear transition from oscillatory to amplified behavior corresponds to the I I symmetry breaking transition.

exponential dynamics. This is the basis of the *PT* symmetry breaking transition which we now explore in further detail.

Figure 4 displays the time response of I versus detuning for three different pump strengths. For clarity, the grayscale plots are normalized to emphasize small amplitude features. The normalization factor (S) is depicted in the top panels. Figure 4(a) displays the response at low pump amplitude, where the gain is small. We observe oscillation of I in time, with a frequency consistent with the detuning. As the pump strength is increased [Figs. 4(b) and 4(c)] we observe a clear transition from oscillatory to nonoscillatory dynamics as the absolute value of the detuning is decreased. The evolution of I vs Q for select detunings is shown in the associated side panels; these plots also highlight how there are values of the detuning where the dynamics are alternately oscillatory or nonoscillatory.

The observed data are in reasonable agreement with a simple model that takes into account the self-Kerr nonlinearity (χ) and the probe signal at the Hamiltonian level,

$$H = \delta a^{\dagger} a + i \frac{\nu}{2} (a^{\dagger 2} - a^2) - \chi a^{\dagger 2} a^2 + i \lambda (a^{\dagger} - a).$$
 (7)

Here, λ is the probe signal strength. To model the amplifier dynamics, we initialize the oscillator in its ground state [i.e., $|\psi(0)\rangle = |0\rangle$] and let the state evolve under the influence of the Hamiltonian [Eq. (7)]. We model the effect of the output port by adding a Lindblad dissipator term $\sqrt{\kappa}a$, where $\kappa/2\pi=0.19$ MHz is determined from the measured quality factor of the device. We use the QUTIP [42,43] master equation solver to obtain the time evolution of I and Q for different detunings. The input drive starts acting on the

amplifier at t = 0 at the same time three-wave mixing is also turned on. From the time evolution of the I quadrature we fit the evolution to the function $A(t) = A_0 e^{-\alpha t} \sin(\omega t + \phi) + A_1$ to determine the frequency of oscillation ω , which is displayed in the lowest panel. We apply the same analysis to the experimental data, where we seed the fit with initial guesses based on the results of the model. In practice, the fits which involve values of α and ω on the same order, are rather unconstrained (as indicated by the large estimated errors of the fits) and the analysis only demonstrates that the data are consistent with the model. We tune the model's relative value of χ to achieve the best agreement with the experimental data. This fit yields a self-Kerr value of approximately $\chi/2\pi = 0.095$ MHz and three different pump strengths as $v/2\pi = 0.013$, 0.046, and 0.072 MHz. For comparison, we also display the associated eigenvalues of Eq. (6) based on the extracted values of ν from the model.

The data exhibit asymmetry about zero detuning that arises due to the presence of the self-Kerr term in the Hamiltonian (7). The self-Kerr energy always decreases the resonance frequency, causing this term to dominate at the negative detuning values. Future work that strives to probe quantum correlations and entanglement in the output modes of the amplifier [24] may have to adopt strategies to reduce the self-Kerr of such amplifier devices [44].

Our work establishes a connection between the transient dynamics of Josephson parametric amplifiers and the celebrated physics of the *PT* symmetry breaking transition. In the context of optical devices, *PT* symmetry and exceptional points have had a profound impact, demonstrating a broad range of devices and functionalities. Future exploration of

exceptional points with Josephson circuits can focus on quantum correlations and noise features in proximity to exceptional points, with applications in sensing and quantum information processing.

We thank Réouven Assouly, Yuxin Wang, Aashish Clerk, and Yogesh Joglekar for their helpful comments. This research

was supported by NSF Grant No. PHY-1752844 (CAREER), the Air Force Office of Scientific Research (AFOSR) Multidisciplinary University Research Initiative (MURI) Award on Programmable systems with non-Hermitian quantum dynamics (Grant No. FA9550-21-1-0202), ONR Grant No. N00014-21-1-2630, and the Institute of Materials Science and Engineering at Washington University.

- [1] C. M. Bender and S. Boettcher, Real spectra in non-Hermitian Hamiltonians having \mathcal{PT} symmetry, Phys. Rev. Lett. **80**, 5243 (1998).
- [2] R. El-Ganainy, K. G. Makris, M. Khajavikhan, Z. H. Musslimani, S. Rotter, and D. N. Christodoulides, Non-Hermitian physics and PT symmetry, Nat. Phys. 14, 11 (2018).
- [3] A. Guo, G. J. Salamo, D. Duchesne, R. Morandotti, M. Volatier-Ravat, V. Aimez, G. A. Siviloglou, and D. N. Christodoulides, Observation of PT-symmetry breaking in complex optical potentials, Phys. Rev. Lett. 103, 093902 (2009).
- [4] C. E. Rüter *et al.*, Observation of parity–time symmetry in optics, Nat. Phys. **6**, 192 (2010).
- [5] B. Peng *et al.*, Parity-time-symmetric whispering-gallery microcavities, Nat. Phys. **10**, 394 (2014).
- [6] H. Hodaei, M.-A. Miri, M. Heinrich, D. N. Christodoulides, and M. Khajavikhan, Parity-time-symmetric microring lasers, Science 346, 975 (2014).
- [7] J. M. Zeuner, M. C. Rechtsman, Y. Plotnik, Y. Lumer, S. Nolte, M. S. Rudner, M. Segev, and A. Szameit, Observation of a topological transition in the bulk of a non-Hermitian system, Phys. Rev. Lett. 115, 040402 (2015).
- [8] J. Li *et al.*, Observation of parity-time symmetry breaking transitions in a dissipative Floquet system of ultracold atoms, Nat. Commun. **10**, 855 (2019).
- [9] L. Xiao *et al.*, Observation of topological edge states in parity-time-symmetric quantum walks, Nat. Phys. **13**, 1117 (2017).
- [10] Ş. K. Özdemir, S. Rotter, F. Nori, and L. Yang, Parity–time symmetry and exceptional points in photonics, Nat. Mater. 18, 783 (2019).
- [11] M.-A. Miri and A. Alù, Exceptional points in optics and photonics, Science **363**, eaar7709 (2019).
- [12] J. Wiersig, Enhancing the sensitivity of frequency and energy splitting detection by using exceptional points: Application to microcavity sensors for single-particle detection, Phys. Rev. Lett. 112, 203901 (2014).
- [13] H. Hodaei *et al.*, Enhanced sensitivity at higher-order exceptional points, Nature (London) **548**, 187 (2017).
- [14] W. Chen, Ş. K. Özdemir, G. Zhao, J. Wiersig, and L. Yang, Exceptional points enhance sensing in an optical microcavity, Nature (London) 548, 192 (2017).
- [15] H. Xu, D. Mason, L. Jiang, and J. G. E. Harris, Topological energy transfer in an optomechanical system with exceptional points, Nature (London) 537, 80 (2016).
- [16] M. Naghiloo, M. Abbasi, Y. N. Joglekar, and K. W. Murch, Quantum state tomography across the exceptional point in a single dissipative qubit, Nat. Phys. 15, 1232 (2019).
- [17] W. Chen, M. Abbasi, Y. N. Joglekar, and K. W. Murch, Quantum jumps in the non-Hermitian dynamics of a superconducting qubit, Phys. Rev. Lett. **127**, 140504 (2021).

- [18] W. Chen, M. Abbasi, B. Ha, S. Erdamar, Y. N. Joglekar, and K. W. Murch, Decoherence-induced exceptional points in a dissipative superconducting qubit, Phys. Rev. Lett. 128, 110402 (2022).
- [19] M. Abbasi, W. Chen, M. Naghiloo, Y. N. Joglekar, and K. W. Murch, Topological quantum state control through exceptional-point proximity, Phys. Rev. Lett. 128, 160401 (2022).
- [20] K. Wang *et al.*, Experimental realization of continuous-time quantum walks on directed graphs and their application in PageRank, Optica 7, 1524 (2020).
- [21] Y. Wu *et al.*, Observation of parity-time symmetry breaking in a single-spin system, Science **364**, 878 (2019).
- [22] W. Liu, Y. Wu, C.-K. Duan, X. Rong, and J. Du, Dynamically encircling an exceptional point in a real quantum system, Phys. Rev. Lett. **126**, 170506 (2021).
- [23] A. A. Clerk, M. H. Devoret, S. M. Girvin, F. Marquardt, and R. J. Schoelkopf, Introduction to quantum noise, measurement, and amplification, Rev. Mod. Phys. 82, 1155 (2010).
- [24] Y.-X. Wang and A. A. Clerk, Non-Hermitian dynamics without dissipation in quantum systems, Phys. Rev. A **99**, 063834 (2019).
- [25] J. Aumentado, Superconducting parametric amplifiers: The state of the art in Josephson parametric amplifiers, IEEE Microw. Mag. 21, 45 (2020).
- [26] T. Yamamoto *et al.*, Flux-driven Josephson parametric amplifier, Appl. Phys. Lett. **93**, 042510 (2008).
- [27] M. A. Castellanos-Beltran, K. D. Irwin, G. C. Hilton, L. R. Vale, and K. W. Lehnert, Amplification and squeezing of quantum noise with a tunable Josephson metamaterial, Nat. Phys. 4, 929 (2008).
- [28] A. Clerk, Introduction to quantum non-reciprocal interactions: From non-Hermitian Hamiltonians to quantum master equations and quantum feedforward schemes, SciPost Phys. Lect. Notes 44, 9 (2022).
- [29] H.-K. Lau and A. A. Clerk, Fundamental limits and non-reciprocal approaches in non-Hermitian quantum sensing, Nat. Commun. 9, 4320 (2018).
- [30] J. C. Budich and E. J. Bergholtz, Non-Hermitian topological sensors, Phys. Rev. Lett. **125**, 180403 (2020).
- [31] R. Shindou, R. Matsumoto, S. Murakami, and J.-i. Ohe, Topological chiral magnonic edge mode in a magnonic crystal, Phys. Rev. B **87**, 174427 (2013).
- [32] V. Peano, M. Houde, C. Brendel, F. Marquardt, and A. A. Clerk, Topological phase transitions and chiral inelastic transport induced by the squeezing of light, Nat. Commun. 7, 10779 (2016).
- [33] V. Peano, M. Houde, F. Marquardt, and A. A. Clerk, Topological quantum fluctuations and traveling wave amplifiers, Phys. Rev. X 6, 041026 (2016).

- [34] W. Chen, D. Leykam, Y. Chong, and L. Yang, Nonreciprocity in synthetic photonic materials with nonlinearity, MRS Bull. **43**, 443 (2018).
- [35] C. Gneiting, A. Koottandavida, A. V. Rozhkov, and F. Nori, Unraveling the topology of dissipative quantum systems, Phys. Rev. Res. 4, 023036 (2022).
- [36] H. Nasari, G. G. Pyrialakos, D. N. Christodoulides, and M. Khajavikhan, Non-Hermitian topological photonics, Opt. Mater. Express 13, 870 (2023).
- [37] A. Blais, A. L. Grimsmo, S. Girvin, and A. Wallraff, Circuit quantum electrodynamics, Rev. Mod. Phys. 93, 025005 (2021).
- [38] M. Kjaergaard *et al.*, Superconducting qubits: Current state of play, Annu. Rev. Condens. Matter Phys. 11, 369 (2020).
- [39] K. W. Murch, R. Vijay, I. Barth, O. Naaman, J. Aumentado, L. Friedland, and I. Siddiqi, Quantum fluctuations in the chirped pendulum, Nat. Phys. 7, 105 (2011).
- [40] Q.-M. Chen, M. Fischer, Y. Nojiri, M. Renger, E. Xie, M. Partanen, S. Pogorzalek, K. G. Fedorov, A. Marx, F. Deppe,

- and R. Gross, Quantum behavior of the Duffing oscillator at the dissipative phase transition, Nat. Commun. 14, 2896 (2023).
- [41] L. Planat, R. Dassonneville, J. Puertas Martínez, F. Foroughi, O. Buisson, W. Hasch-Guichard, C. Naud, R. Vijay, K. Murch, and N. Roch, Understanding the saturation power of Josephson parametric amplifiers made from SQUID arrays, Phys. Rev. Appl. 11, 034014 (2019).
- [42] J. Johansson, P. Nation, and F. Nori, QuTiP: An open-source Python framework for the dynamics of open quantum systems, Comput. Phys. Commun. **183**, 1760 (2012).
- [43] J. Johansson, P. Nation, and F. Nori, QuTiP 2: A Python framework for the dynamics of open quantum systems, Comput. Phys. Commun. **184**, 1234 (2013).
- [44] N. E. Frattini, V. V. Sivak, A. Lingenfelter, S. Shankar, and M. H. Devoret, Optimizing the nonlinearity and dissipation of a SNAIL parametric amplifier for dynamic range, Phys. Rev. Appl. 10, 054020 (2018).